Impact of sedimentary degradation and deep water column production on GDGT abundance and distribution in surface sediments in the Arabian Sea: Implications for the TEX_{86} paleothermometer

Sabine K. Lengger[#, *], Ellen C. Hopmans, Jaap S. Sinninghe Damsté and Stefan Schouten

Department of Marine Organic Biogeochemistry, Royal NIOZ Netherlands Institute for Sea Research, P. O. Box 59, 1790AB Den Burg, Texel, The Netherlands.

[#] Present address: WA Organic and Isotope Geochemistry Centre, Department of Chemistry, Curtin University, GPO Box U1987, Perth, WA 6845, Australia.

*Corresponding author. E-mail address: sabine.lengger@curtin.edu.au

Abstract

The TEX_{86} is a widely used paleotemperature proxy based on isoprenoid glycerol dibiphytanyl glycerol tetraethers (GDGTs) produced by Thaumarchaeota. Archaeal membranes are composed of GDGTs with polar head groups (IPL-GDGTs), most of which are expected to be degraded completely or transformed into more recalcitrant core lipid (CL)-GDGTs upon cell lysis. Here, we examined the differences in concentration and distribution of core lipid (CL)- and intact polar lipid (IPL)-GDGTs in surface sediments at different deposition depths, and different oxygen bottom water concentrations (<3 to 83 $\mu mol \cdot L^{-1}$). Surface sediments were sampled from 900 to 3000 m depth on a seamount (Murray Ridge), whose summit protrudes into the oxygen minimum zone of the Arabian Sea. Concentrations of organic carbon, IPL- and CL-GDGTs decreased linearly with increasing maximum residence time in the oxic zone of the sediment (t_{OZ}), suggesting increasing sedimentary degradation of organic matter and GDGTs. IPL-GDGT-0 was the only exception and increased with t_{OZ}, indicating that this GDGT was probably produced in situ in the surface sediment. Concentrations of crenarchaeol with glycosidic headgroups decreased with increasing t_{OZ}, while crenarchaeol with a hexose, phosphohexose head (HPH) group, in contrast, showed an increase with increasing t_{OZ}, indicating that the concentration of HPH crenarchaeol was primarily determined by in situ production in surficial sediments. TEX_{86} values of both IPL-derived GDGTs and CL-GDGTs decreased by ~0.08 units with increasing water depth, in spite of the sea surface temperatures being identical for the restricted area studied. In situ production in sediments could be excluded as the main cause, due to the slow production rates of GDGTs in sediments, and previous observations of the same trends in TEX_{86} in sediment trap material. Instead, the incorporation of GDGTs produced in the oxygen minimum zone (with high TEX_{86} values) and their preferential degradation during the sinking through the water column, or differential degradation of IPL-GDGTs per head group could be the causes for the observed change in TEX_{86} values. The effect of differential degradation might cause differences between oxic and anoxically deposited sediments, and, together with a potential deep water contribution on TEX_{86} values, could translate into changes in reconstructed temperature of <3°C, which might have to be accounted for in TEX_{86} calibration and paleotemperature studies of deep water sedimentary records.

1. Introduction

The TEX_{86} is a paleotemperature proxy that has been developed over the last decade. Schouten et al. (2002) discovered a relationship of ring distributions of common archaeal membrane lipids, isoprenoid glycerol dibiphytanyl glycerol tetraethers (GDGTs, Fig. 1), with sea surface temperature and quantified this, using a ratio of four different GDGTs, called the TEX_{86}. These specific compounds have been shown to be mainly produced by Thaumarchaeota in the marine environment (Sinninghe Damsté et al., 2002a; 2002c). They are present in the cell membranes of live cells as intact polar lipids (IPLs), with polar head groups such as hexose- and phosphate-groups (Schouten et al., 2008; Pitcher et al., 2010; 2011). These IPL-GDGTs were generally assumed to be associated only with living and active cells (Biddle et al., 2006; Lipp et al., 2008; Lipp and Hinrichs, 2009; Schubotz et al., 2009). There is, however, an increasing amount of evidence that IPL-GDGTs, and especially those with glycosidic headgroups, can be preserved over geological timescales, especially under anoxic conditions (Harvey et al., 1986; Schouten et al., 2010; Liu et al., 2011; Logemann et al., 2011; Lin et al., 2013; Lengger et al., 2012a; 2013; Xie et al., 2013).

For the TEX_{86}, a global calibration was developed based on marine surface sediments (Kim et al., 2008) and recently, two calibrations for two GDGT ratios were proposed – one for tropical/subtropical and one for polar oceans, the TEX^{H}_{86} and the TEX^{L}_{86} (Kim et al., 2010), respectively. The TEX_{86} proxy is now widely used to reconstruct paleotemperatures of the sea surface using ancient marine sediments (e.g. Liu et al., 2009; Forster et al. 2007). However, even though the TEX_{86} is strongly related to sea surface temperature, an equally strong relation with temperatures from 0-200 m water depth is observed (Kim et al., 2008; 2012). Indeed, it was shown in several areas that the TEX_{86} temperatures reflect subsurface temperatures (Ingalls et al., 2006; Huguet et al., 2007; Lopes dos Santos et al., 2010; Kim et al., 2012; Nakanishi et al., 2012). Molecular ecological studies have shown that Thaumarchaeota are not only present in the upper 200 m of the marine water column but also deeper in the water column, although their cell numbers generally decrease with depth (e.g. Karner et al., 2001; Herndl et al., 2005; Agogué et al., 2008; Reinthaler et al., 2010). The reason why most of the GDGTs present in marine surface sediments may still derive from the upper 0-200 m could be the

preferential packaging of these GDGTs into fecal pellets and marine snow (Wakeham et al., 2003; Wuchter et al., 2005; Huguet et al., 2006a). This process mainly takes place in and just below the photic zone as this is, due to high abundance of phytoplankton, the habitat for zooplankton and thus the most active food web (ibid.). Below the photic zone, the grazing organisms have to rely on sinking particles and chemoautotrophic production of prokaryotic biomass. Thus, the food web activity, and presumably fecal pellet packaging, is much reduced (Burd et al., 2010). However, the TEX_{86} values of material collected in sediment traps suggest that there may be a contribution of archaea from the deeper water column, i.e. >200m (Wuchter et al., 2006; Turich et al., 2007). Indeed, radiocarbon analysis of sedimentary GDGTs suggested a contribution of deep water-dwelling archaea (>200 m) to the sedimentary GDGTs, estimated to be as high as 100% (Pearson et al., 2001), 83% (Ingalls et al., 2006) and 74 to 100% (Shah et al., 2008). Recently, Taylor et al. (2013) attributed differences in TEX_{86} in global sediments and the sediment record to differences in GDGT distributions with water depth. Nonetheless, the TEX_{86} from surface sediments collected from all over the world shows a robust correlation with sea surface temperatures (Kim et al., 2008; Kim et al., 2010). Furthermore, Basse et al. (2014) observed that GDGTs produced in nepheloid layers between 200 and 750 m water depth in an oxygen minimum zone were degraded preferentially over surface-derived GDGTs in the oxic water column, resulting in mainly surface derived GDGTs being preserved in the underlying sediments. Thus, it remains unknown to what extent sedimentary GDGTs derive from deeper water-dwelling archaea. This makes it hard to constrain the potential bias of deeper water production on TEX_{86} paleothermometry.

Additionally, a bias of the TEX_{86} could arise from preferential degradation of specific GDGTs. Degradation under oxic conditions can be caused by a number of different factors related to oxygen, such as primary production rate, sediment accumulation rate, bottom water oxygen concentration, availability of O_2 and other dissolved electron acceptors, microbial dynamics, mixing and irrigation by macrobenthos, or redox fluctuation and has thus been labelled the “oxic effect” (Hedges et al., 1999; Keil et al., 1994; Keil and Cowie, 1999). It has been shown to cause a decrease in TEX_{86} in re-oxidized turbidite sediments as preferential degradation of marine over soil-derived isoprenoid GDGTs revealed a terrestrial signal (Huguet et al., 2009). Lengger et al. (2013) recently showed that

97 the TEX_{86} of IPL-, but not CL-GDGTs, changes substantially by post-depositional oxidation through
98 the differential degradation of IPL-GDGTs with different head groups. Short-term degradation by
99 exposure of anoxically deposited sediments to an oxic water column, showed no significant impact on
100 the TEX_{86} of CL-GDGTs (Kim et al., 2009). Schouten et al. (2004), who compared the TEX_{86} of
101 oxically and anoxically deposited sediments, also found no differences between them. The studies by
102 Huguet et al. (2009) and Kim et al. (2009), however, showed the impact of short term (1 year) or long
103 term (>10 kyr) degradation, and Schouten et al. (2004) compared the TEX_{86} of sediment deposited at
104 different times and different environmental conditions. The impact of degradation under oxic
105 conditions on intermediate time scales is not clear.

106 To address the issues of degradation as well as the depth origin of sedimentary GDGTs, we examined
107 surface sediments from the Murray Ridge in the Northern Arabian Sea. The Murray Ridge is a steep
108 ridge that impinges the vast oxygen minimum zone (OMZ) that the Arabian Sea possesses. It thus
109 allows the sampling of surface sediments that principally receive the same particle flux from the base
110 of the photic zone, but at a wide range of water depths (900 – 3000 m) and bottom water oxygen
111 concentrations (<3 to 83 $\mu mol \cdot L^{-1}$). An earlier, limited study of three surface sediments at 900, 1300
112 and 3000 m water depth showed that concentrations of CL- and IPL-derived GDGTs as well as IPL-
113 crenarchaeol species were decreasing with increasing water depth and thus bottom water oxygen
114 concentrations, but also illustrated that the TEX_{86} values of both CL- and IPL-derived GDGTs were
115 decreasing (Lengger et al., 2012a). It was speculated that part of the GDGTs in the sediment originated
116 not only from the surface waters but also, in part, from the deeper waters. An alternative explanation
117 offered was the differential degradation of IPL-GDGTs, as they were shown to have different TEX_{86}
118 values dependent on the nature of the head group. In order to investigate the causes of this apparent
119 depth trend, here, we substantially extended our previous study by analyzing IPL- and CL-GDGT
120 concentrations and distributions in ten surface sediments (0-0.5 cm) from the Murray Ridge, collected
121 at regular intervals between 900 to 3000 m water depths. As we suggested earlier that the distribution
122 of headgroups of IPL-GDGTs was affecting the TEX_{86} (Lengger et al., 2012a), IPL-GDGTs from
123 surface sediment (0-2 cm) and deeper sediment (20-24 cm) from cores recovered from the water
124 depths 900, 1300 and 3000 m were separated according to head groups, quantified, and their GDGT-

distribution was investigated. The results were used to determine the impact of time spent under oxic conditions on the concentrations and distributions of sedimentary IPL- and CL-GDGTs and to investigate the contribution of deep water Thaumarchaeota to the GDGT-pool and the impact on the TEX_{86} in surface sediments.

2. Materials and Methods

2.1. Sampling

Surface sediments were taken from multicores in the Northern Arabian Sea along a transect of the Murray Ridge during the PASOM cruise (64PE301) in January 2009 (Fig. 2, Table 1). The sediment cores, of 20 to 36 cm length, were sliced on board the *R/V Pelagia* in 0.5 to 4 cm intervals and stored in geochemical bags, frozen immediately at -80°C and further transported and stored at -20°C. Prior to analysis, the sediment was freeze-dried and homogenized. Surface sediment (0-0.5 cmbsf), as used in TEX_{86} core-top calibrations, was used for all measurements, except for the semi-preparatory HPLC, where a mixture of the top 0-2 and 20-24 cmbsf were used. Oxygen concentrations of the water column were measured by an SBE 43 dissolved oxygen sensor (Seabird, WA, USA) fitted to the CTD frame and calibrated against Winkler titrations. The limit of detection for these methods was 3 µmol · L^{-1}. Oxygen penetration depths were measured on board in 0.1 mm resolution using an OX-100 micro sensor (Unisense AS, Aarhus, DK) with a guard cathode as described by Revsbech (1989). The Murray Ridge sediment cores have been described previously by Kraal et al. (2012), who reported pore water profiles and the inorganic geochemistry of the depositional settings, and Koho et al. (2013), who reported evidence for the dependence of organic carbon concentrations and organic matter quality on oxygen, macrofaunal activity and microbial biomass.

2.2. Organic carbon concentrations, sedimentation rates and residence time in the oxic zone

Freeze-dried sediments were analyzed for organic carbon concentrations (C_{org}). The freeze-dried sediment was acidified over night with 2N HCl, subsequently washed with bidistilled H_2O and the water was removed by freeze-drying. The decalcified sediments were measured on a Flash EA 1112 Series (Thermo Scientific) analyzer coupled via a Conflo II interface to a Finnigan Delta^{plus} mass spectrometer. Standard deviations from three measurements ranged from 0.01 to 0.2 % total organic carbon (TOC).

As described by Lengger et al. (2012a) for the cores at P900, P1300 and P3000, and Koho et al. (2013) for all cores, determination of the sedimentation rates was carried out by ^{14}C dating. The maximum

residence time the organic matter at 0.5 cm spent in the oxic zone (t_{OZ}, Eq. 1) was calculated from the oxygen penetration depth (OPD, [mm]) and the sediment accumulation rates (SAR, [mm.kyr^{-1}]). In some of the cores oxygen penetrated rather deeply, but since we only used the upper 5 mm of the core for TOC, CL- and IPL-GDGT determination, as used in TEX_{86} core top calibrations, we used the 5 mm instead of the full oxygen penetration depth:

$$t_{OZ} = \frac{\min(OPD,5)}{SAR} \quad \text{(Eq. 1).}$$

This t_{OZ} is mathematically similar to oxygen exposure time as defined by Hartnett et al. (1998). However, Hartnett et al. (1998) used oxygen exposure time to investigate factors impacting organic matter burial fluxes *below* the oxygen penetration depth. Here, we use it to determine the dependence of concentrations of organic matter and GDGTs in surface sediments on the time it has spent under oxic conditions. Uncertainties in the t_{OZ} values mainly arise from the uncertainties in sedimentation rates, as outlined by Koho et al. (2013).

2.3. Sediment extraction and separations

Aliquots (1-2 g) of freeze-dried surface sediment (0-0.5 cm sediment depth) were extracted with a modified Bligh and Dyer procedure as described previously by Pitcher et al. (2009). Briefly, extraction with methanol (MeOH)/dichloromethane (DCM)/phosphate buffer (PB) 50 mM, pH 7.5 (2:1:0.8, v/v/v) was carried out three times by ultrasonication and the supernatant was collected after centrifugation and combined, then adjusted to a solvent ratio of MeOH/DCM/PB of 1:1:0.9 (v/v) resulting in phase separation between the DCM and the MeOH/PB. The DCM phase was collected and the MeOH/PB mixture was extracted twice more with DCM. The combined DCM phases were reduced with a rotary evaporator, re-dissolved in DCM/MeOH 9:1 (v/v), filtered over cotton wool and subsequently dried under a stream of N_2. The extract was stored at -20°C.

An aliquot was fractionated over a silica column in order to separate the IPL from the core lipids (CL) following the procedure of Oba et al. (2008), as modified by Lengger et al. (2012b). Briefly,

fractionation was achieved over a silica column using 6 column volumes hexane/ethyl acetate 1:1 (v/v; CL-GDGTs) and 10 column volumes MeOH (IPL-GDGTs). Quantification was achieved by adding 0.1 μg C_{46}-GDGT internal standard (Huguet et al., 2006b) to the fractions. An aliquot of the IPL-GDGT fraction was transferred to a vial, dried and stored frozen for quantification of core lipids which eluted in the intact polar lipid fraction ("carry over"). These were typically <2% of the GDGTs present in CL fraction or 10% of GDGTs present in the IPL fraction. The remaining IPL-fraction was subjected to hydrolysis to release CL-GDGTs (=IPL-derived GDGTs).

In order to compare TEX_{86} values of the surface sediments with those of surface sediments in other studies, we analyzed the TEX_{86} values of the surface sediments using standard extraction and separation methods used for calibration of the TEX_{86} index (Kim et al., 2008; Kim et al., 2010). Aliquots of a few hundred mg of freeze-dried surface sediment were extracted after addition of pre-extracted diatomaceous earth in an Accelerated Solvent Extractor 200 (ASE 200, DIONEX, CA, USA) with a mixture of DCM/MeOH 9:1 v:v at 100 °C and $7.6 \cdot 10^6$ Pa. The polar GDGTs were separated from the apolar fraction by silica gel column chromatography (Al_2O_3, three column volumes hexane/DCM 9:1 for the apolar and 4 column volumes DCM/MeOH 1:1 for the polar fraction).

2.4. Semi-preparative HPLC

For the isolation of particular IPL-GDGTs, repetitive semi-preparative HPLC was used as described and carried out previously for P1300 (Lengger et al., 2012a) for sediments from stations P900, P1300 and P3000, of sediment from 0-2 cm depth ("top") and 20-24 cm depth ("bottom"). The fractions containing the intact polar lipids, i.e. monohexose (MH)-crenarchaeol, dihexose (DH)-crenarchaeol and hexose, phosphohexose (HPH)-crenarchaeol, as detected by electrospray ionization mass spectrometry in selected reaction monitoring mode (Pitcher et al., 2011), were pooled. To these six fractions, i.e. containing monohexose-GDGTs, dihexose-GDGTs and hexose, phosphohexose-GDGTs, and the combined eluted fractions between those, 0.1 μg C_{46}-GDGT internal standard was added. The dihexose-GDGTs likely contained a minor amount of co-eluting hydroxyl-GDGTs (Liu et al., 2012), as observed in *Candidatus* 'Nitrosopumilus maritimus' SCM1 and previously described as "unknown + 180" (Schouten et al., 2008). All fractions were acid-hydrolyzed and the specific IPL-derived GDGT

distributions were quantified using HPLC/APCI-MS and the C_{46}-GDGT internal standard method as described above.

2.5. *HPLC/APCI-MS*

Analysis of CL-GDGTs and IPL-derived GDGTs concentrations by HPLC/APCI-MS and calculation of TEX_{86} was carried out as described previously, using response factors as determined by a 1:1 (wt/wt) C_{46}-GDGT / crenarchaeol mixture (Schouten et al., 2012). Reproducibility for TEX_{86} values is typically < 0.02, corresponding to errors of < 1 °C (Schouten et al., 2007). Temperatures were calculated according to the calibrations according to Kim et al. (2010) for TEX^{H}_{86}.

3. Results

3.1. Sedimentation rate, organic carbon concentration and residence time in the oxic zone

Sedimentation rates for the ten cores ranged from 26 to 134 mm · kyr^{-1}, and were high at stations in and just below the OMZ, and lower at the deeper stations (Table 1). No sedimentation rate could be obtained for P1500 due to a constant age throughout the core (Koho et al., 2013). Furthermore, the sedimentation rate for station P3000 was unusually high (83 mm · kyr^{-1}), disagreeing with the ^{210}Pb profile, which can be explained by lateral transport probably affecting the sediment at this station, causing the surface sediment to appear older. Therefore, the sedimentation rates of these two stations were not used in this study. Organic carbon concentrations (C_{org}) decreased steadily with depth from 60 to 10 mg · g sed dw^{-1}, while bottom water oxygen concentrations increased with depth (from 3 μmol · L^{-1} to 83 μmol · L^{-1} ; Fig. 3a; Table 1). Oxygen penetration depths (OPD) increased from 0.125 mm at P900 to 18 mm at P3000 (Table 1), resulting in an increase with water depth of the maximum residence time that the top 0.5 cm sediment slice has spent under oxic conditions (t_{OZ}), initially strongly from 1 yr to 152 yr between stations P900 and P1400, and subsequently more slowly from 152 to 192 yr between stations P1400 and P2500 (Fig. 3b, Table 1).

3.2. Concentrations and TEX_{86} values of GDGTs

CL- and IPL-GDGT concentrations in the surface (0-0.5 cm) sediments generally decreased with increasing water depth (Fig. 4a-b; Table A1). CL-GDGT concentrations were 7.7 and 55 μg ·

g sed dw^{-1} for GDGT-0 and crenarchaeol, respectively, in the shallowest sediment and 0.25 and 0.67 μg · g sed dw^{-1}, respectively, in the surface sediment from the greatest depth (Fig. 4a). The isoprenoid GDGTs used in the TEX_{86} palaeothermometer (i.e. GDGT-1, -2, -3 and the crenarchaeol regioisomer; iGDGTs) had summed concentrations of 15 μg · g sed dw^{-1} at the shallowest station, decreasing to values of 0.22 μg · g sed dw^{-1} at the deepest station (Fig. 4a). IPL-derived GDGTs were present in much lower concentrations compared to CL-GDGTs; i.e. 0.14 – 1.1 μg · g sed dw^{-1} for GDGT-0, 0.1 – 3.1 μg · g sed dw^{-1} for crenarchaeol, and 0.04 – 1.7 μg · g sed dw^{-1} for the sum of the other i-GDGTs, with declining concentrations with increasing water depth (Fig. 4b). IPL-derived GDGTs corresponded to 10 to 20% of CL-GDGTs for all isomers except for GDGT-0, which showed IPL/ CL ratios of > 30% at water depths > 1000 m (Fig. 4c).

The TEX_{86} values for the CL-GDGT fraction decreased with increasing water depth from 0.78 at Station P900 to 0.72 at Station P3000 (Fig. 4d, Table A2). IPL-derived GDGTs showed a similar trend, with TEX_{86} values of 0.78-0.80 decreasing to 0.72. In order to compare these results to paleotemperature studies, which typically do not use Bligh and Dyer extractions and IPL/CL separations as used here, we also performed ASE extraction, followed by a chromatographic separation and analysis of the obtained polar fraction. The TEX_{86} values thus obtained (Fig. 4d) are comparable to the TEX_{86} values measured on the CL-fraction within the range of the analytical error (0.02 units).

3.3. Individual IPL GDGTs in Arabian Sea surface sediments

As there is evidence that degradation behavior of IPL-ether lipids differs depending on their head group composition (Harvey et al., 1986; Lengger et al., 2012a; 2013), we separated IPL-GDGTs from three stations according to their head group composition using semi-preparatory HPLC. This allowed investigation of differences in degradation behavior and how this influences the TEX_{86}. For quantification of all IPL-GDGTs with different headgroups, preparatory HPLC was the most accurate available method. The fractions containing the IPL-GDGTs (MH-, DH- and HPH-derived GDGTs) were subsequently hydrolyzed and the obtained core lipids were quantified. This procedure was used with sediments of the top 0-2 cm and from 20-24 cm sediment depth for three different water depths

(900, 1300 and 3000 m) (Fig. 5a, left panels; Table A3). Preliminary results of sediment from P1300, 0-2 and 20-24 cm, have already been described earlier (Lengger et al., 2012a), i.e. the TEX_{86} values of the released GDGTs. For this study, IPL-GDGT concentrations were also quantified.

The isolation of individual IPLs showed that IPL-GDGT concentrations were highest in the surface sediment from shallow water depth compared to those from greater water depth (Fig. 5a, left panels), consistent with the IPL-GDGT concentration profiles (Fig. 4b). MH-derived GDGTs dominated, but DH-derived GDGTs were present in high proportions as well (Fig 5a, left panels). HPH-derived GDGTs were present in increasingly higher absolute abundance with increasing water depth with HPH-derived GDGTs at station P3000 representing the most abundant form of IPL-GDGTs. The deeper sediments (20-24 cm) showed MH- and DH-derived concentrations similar to the surface sediments but a much lower concentration of HPH-derived GDGTs was evident, especially for station P3000 (Fig. 5a, left panels).

The distribution of core lipid GDGTs showed substantial differences for the different collected IPL fractions; i.e. DH contained a much higher fractional abundance of GDGT-1, -2, -3, and the crenarchaeol isomer than MH and HPH (right panels in Fig. 5a). Some smaller differences were observed when these GDGT distributions per specific IPL group were compared for the surface (0-2 cm) and deeper (20-24 cm) sediments (right panels in Fig. 5a).

These differences were also reflected in the TEX_{86} values of the different IPL fractions (Fig. 5b). DH-derived GDGTs always showed the highest, and MH-derived GDGTs intermediate TEX_{86} values, i.e. 0.80 - 0.90 for the DH-derived GDGTs and 0.60 - 0.72 for the MH-derived GDGTs (Fig. 5b). These values decreased for both MH- and DH-derived GDGTs with water depth but not with depth in the sediment. For HPH-derived GDGTs, TEX_{86} values in the surface (0-2 cm) sediments of stations P1300 and P3000 only could be reliably determined as concentrations were too low in the other sediments. Distributions are shown in Fig. 5a, but it is obvious that they mainly consist of GDGT-0 and crenarchaeol, and the minor i-GDGTs are not present in high amounts. HPH-derived GDGTs showed the lowest TEX_{86} values, i.e. 0.37 - 0.42, much lower than those of the MH and DH IPLs (Fig. 5b). Weighted-average TEX_{86} values (Total; Fig. 5b) were calculated from the absolute abundances of the

MH-, DH- and HPH-IPL and their GDGT composition. These values are similar to the average TEX_{86} values of the IPL-GDGT of the top 0-2 cm, as calculated from values of the different sediment layers published previously (Lengger et al., 2012a), confirming that the three major IPLs isolated are quantitatively representative of the total IPL-GDGT pool.

4. Discussion

4.1. Impact of degradation and in situ sedimentary production on GDGT concentrations

Organic carbon concentrations in the surface sediments (0-0.5 cm) are decreasing with increasing water depth, coincident with increasing bottom water oxygen concentrations, increasing oxygen penetration depths, decreasing sedimentation rates and thus longer maximum residence times in the oxic zone (Fig. 3; Table 1). Strikingly, there is a strong linear correlation between C_{org} and t_{OZ} (R^2 0.93; Fig. 6a). This expands on results by Koho et al. (2013), who, in the same sediments, found an exponential relationship between organic carbon content and bottom water oxygen concentrations. Assuming that the organic carbon flux to these sediments was similar at all stations, it suggests that longer times spent under oxic conditions lead to lower organic carbon contents due to degradation associated with these oxic conditions, in agreement with previous observations who held different factors responsible for this "oxic effect" (cf. Hartnett et al. 1998; Hedges et al. 1999; Sinninghe Damsté et al. 2002b; Burdige 2007).

Similarly to C_{org}, CL-GDGT concentrations were also strongly linearly negatively correlated to t_{OZ} (R^2 0.82-0.83), with decreases over depth of 70 – 90 % from P900 to P3000 (Table A1), and crenarchaeol showing the most pronounced decrease with t_{OZ} (Fig. 6c). Remarkably, IPL-derived crenarchaeol and other isoprenoid GDGTs (sum of -1, -2, -3 and the crenarchaeol regioisomer) showed a high correlation (R^2 0.87-0.88) with t_{OZ}, but less so for IPL-derived GDGT-0 (R^2 0.49), which did not decrease in abundance but rather increased when sediment from P3000 is compared to P900. This is a strong indication for in situ production of GDGT-0, which is produced by many archaea (e.g. Koga and Nakano, 2008), not only Thaumarchaeota. Lengger et al. (2012a), who analyzed sediment cores of 24-32 cm length at stations P900, P1300 and P3000 in high (0.5 – 4 cm) resolution, also found a high abundance of GDGT-0 in the surface sediments with oxygenated pore waters (stations P1300, P3000).

The concentrations of IPL-derived GDGT-0 were particularly high for P3000, at 0.5 - 1.5 cm sediment depth. However, interestingly, this high relative abundance was not evident further downcore or in the CL-GDGTs. Lengger et al. (2012a) thus concluded that the in situ-produced IPL-derived GDGT-0 was degraded quickly, as it was probably more bioavailable than the matrix-embedded material transported from the sea surface. The strong correlation of the concentrations of the other IPL-GDGTs with t_{OZ} suggests that degradation under oxic conditions is the predominant factor controlling IPL-GDGT concentrations in the surface sediments. Comparison of the slopes of this correlation, when normalized on initial concentrations, showed that they were similar for all IPL-derived GDGTs, CL-GDGTs and C_{org}, i.e. 0.45-0.54 units (Table 2), except for IPL-derived GDGT-0. This suggests that the concentrations of all these GDGTs (except for GDGT-0) are primarily controlled by degradation.

Semi-preparative HPLC provided quantitative information about the proportions of IPL-GDGTs with different head groups, i.e. MH-, DH- and HPH-derived GDGTs (Fig. 5). This revealed that MH- and DH-derived GDGTs decreased by an order of magnitude with water depth between stations P900 and P3000. The HPH-derived GDGTs showed a different pattern to the MH- and DH-GDGTs, i.e. with increasing water depth, the concentrations actually increased strongly in the surface sediment, suggesting sedimentary in situ production. This increase in HPH-derived GDGTs was mainly responsible for the increase in GDGT-0 in the IPL-derived GDGTs. Previous work suggested that HPH-GDGTs are not preserved to a large extent (Schouten et al. 2010; Lengger et al. 2012a, 2013), and their presence is mainly the result of sedimentary in situ production of Archaea, amongst others most probably Thaumarchaeota involved in nitrification (at least as a source for HPH-crenarchaeol). Indeed, in the sediments from deeper water depths, the organic carbon content is also much lower, resulting primarily from degradation in the surface sediments (Fig. 6a). During this process, ammonium will be generated from organic nitrogen and this, together with the increased oxygen concentration, may provide a niche for benthic Thaumarchaeota in these sediments.

In the deep sediment, concentrations of HPH-GDGTs were lower than those of the surface sediments, suggesting that the surface-produced HPH-GDGTs were not preserved at depth. Contrastingly, for both MH- and DH-GDGTs at P900 and, to some extent, also at P1300, an increase with sediment

depth was noted, which is consistent with data presented by Lengger et al. (2012a). This could potentially indicate in situ production at depth in the sediment, however, as TOC was also elevated in the 20-24 cm sediment sections, it more likely indicates increased preservation at the time of deposition (see discussion in Lengger et al., 2012a). Part of the MH-GDGTs may be the result from the degradation of in situ produced HPH-GDGTs, but as the TEX_{86} values of MH-GDGTs are not substantially decreasing with sediment depth (Fig. 5b), as an addition of HPH-GDGTs with substantially lower TEX_{86} values would entail, this is not likely to be an important process.

4.2. Decrease of TEX_{86} with water depth: causes and implications

An important observation in our study is the decrease of TEX_{86} in surface sediments with increasing water depth in CL- and IPL-derived GDGTs, the MH-GDGTs and DH-GDGTs as well as in the GDGTs obtained by ASE extraction (Fig. 4d, 5b). There are three possible explanations for this decrease with water depth:

(i) An increasing contribution of in situ production of GDGTs in surface sediments with increasing water depth, possibly by benthic Thaumarchaeota, and potentially other archaea, with the former probably dependent on oxygen and thus producing GDGTs to a higher degree in sediments with higher bottom water oxygen concentrations;

(ii) An increasing contribution of GDGTs produced by archaea in the deeper water column in sediments deposited at greater depth. GDGTs produced by deeper water dwelling archaea may have a lower TEX_{86} (Schouten et al., 2012), which may cause the decrease in TEX_{86}.

(iii) Increasing degradation of CL- and IPL-GDGTs in surface sediments with increasing water depth due to the increase in t_{OZ}, resulting in alterations in GDGT distributions.

Regarding explanation (i), this would require that sedimentary Thaumarchaeota are increasingly present and active in the sediments with increasing water depth and that the GDGTs produced by the benthic archaeal population have a different GDGT distribution, i.e. with a lower TEX_{86} value, than that of the descending particles in the water column, in order to cause a linear correlation with an $R^2 > 0.8$. This seems a plausible explanation for these changes since Thaumarchaeota are known for

oxidizing ammonia aerobically, and, accordingly, the abundance of HPH-GDGTs is higher at P3000 than at P1300 and P900 (Fig. 5a). Lengger et al. (2012a), who investigated depth trends in the sediments, also observed anomalous GDGT-distributions and TEX_{86} values as low as 0.65 in the IPL-GDGTs in sediments at 0.5-2 cm depth of core P3000, which was attributed to in situ production, as the distributional changes were occurring starting from 0.5 cm sediment depth. However, these drastic deviations disappeared with increasing depth in the sediment, where TEX_{86} values were again identical to surface values. Furthermore, such "anomalies" in TEX_{86} values were not observed in the CL-GDGT distribution of these surface sediments, thus indicating that in situ production in the sediment is unlikely to be the cause for the decrease in TEX_{86} in the CL-GDGT fraction. Further, recently reported evidence from sediment incubations (Lin et al., 2013; Xie et al., 2013) suggests extraordinarily low growth rates of GDGT-producing archaea (turnover times 1.7 – 20.5 kyr, Lin et al., 2013; 1.6 – 73 kyr, Xie et al., 2013). In situ production in the surface sediment, which was probably deposited in a period of <1 to 200 yrs ago, would therefore likely be minimal. Evidence from settling particles further corroborates this: Wuchter et al. (2006) analyzed fluxes and TEX_{86} values of CL-GDGTs in sediment traps from the Arabian Sea at different water depths (500, 1500 and 3000 m). They noted that the CL-GDGT fluxes and TEX_{86} values in the deepest trap did not show any seasonal trend, as was observed in the 500 m trap, and that the flux-weighted TEX_{86} value in the deepest trap was slightly lower (ca. 0.02) than in the shallowest trap. This suggests that the observed trend of decreasing TEX_{86} value with increasing water depth is already a characteristic of the settling particles and thus likely created in the water column.

Regarding the possibility of option (ii), i.e. that GDGTs from the deeper water column (with a lower TEX_{86} value) are increasingly contributing to the settling flux of GDGTs received by the surface sediments in sediments deposited at greater water depth, which would cause a decrease of the TEX_{86}. This would explain why Wuchter et al. (2006) noted a decrease in TEX_{86} value in the sediment trap at 3000 m compared to that at 500 m, suggesting addition of GDGTs with a lower TEX_{86} in deeper waters. Furthermore, TEX_{86} values of water column SPM samples between 900-2000 m in the Arabian Sea were also decreasing with water depth from 0.78 at 900 m to 0.66 at 2000 m for CL and from 0.81 to 0.65 for IPL-derived GDGTs (Schouten et al., 2012), although these data may only provide a

395 snapshot in time and the SPM analyzed probably consisted of a mixture of sinking and suspended
396 particles. The incorporation of GDGTs from deeper waters into settling particles has been suggested
397 previously based on radiocarbon content and GDGT distributions (Ingalls et al., 2006; Huguet et al.,
398 2007; Turich et al., 2007). This would imply that GDGTs that are being produced by free or particle-
399 associated Archaea in deeper waters are, in part, also exported to the sediment.

400 To examine option (iii), an effect of sedimentary degradation, we correlated TEX_{86} with the t_{OZ} and
401 found a linear relationship (R^2 values 0.68 – 0.95; Fig. 6b). It is thus possible that progressing
402 degradation of GDGTs is, partially, causing the decrease in TEX_{86} with increasing water depth.
403 However, this cannot be the only explanation since it would not explain the observation of Wuchter et
404 al. (2006) that TEX_{86} values in the settling particles decrease with increasing water depth. The short
405 timescales over which settling occurs are likely too short to cause substantial changes in the TEX_{86} by
406 degradation in the water column: Kim et al. (2009) investigated short timescales (1 year) and showed
407 that oxygen exposure of sedimentary GDGTs did not have any effect on TEX_{86} values. Furthermore,
408 the change in TEX_{86} with water depth is visible even in individual IPLs, i.e. the MH- and DH-GDGTs
409 (Fig. 5b). This would imply that degradation rates of IPL-GDGTs are determined by core lipid
410 composition rather than head group, which could only be explained by a different provenance of these
411 IPL-GDGTs, resulting in different degrees of matrix protection (as in terrestrial vs. marine, cf.
412 Middelburg 1989; Huguet et al., 2009; Lengger et al., 2013). However, the organic matter deposited
413 on the Murray Ridge is entirely marine, and it is thus not clear where this difference could originate
414 from.

415 A possible explanation is a scenario similar to that suggested by Basse et al. (2014), who observed a
416 similarly high TEX_{86} in the OMZ off Cape Blacn which progressively disappeared in the oxic waters
417 below the OMZ. Basse et al. (2014) attributed this to the lack of matrix protection of GDGTs
418 produced in the macrofauna-deficient OMZ (potentially on sinking particles), as opposed to the
419 surface-exported GDGTs transported in and protected by fecal pellets. In our case it could mean that
420 the, compared to the surface waters, relatively high TEX_{86} values produced in the waters of the OMZ
421 of the Arabian Sea (Schouten et al., 2012) are preferentially degraded when sinking through the oxic

water column below the OMZ, leading to a lower TEX_{86} (approaching surface values again) with increasing depth. Thus, the decrease in TEX_{86} in the surface sediments with increasing depth of deposition may be due to selective degradation of GDGTs, possibly in combination with the addition of GDGTs produced in the deeper water column. These differences in TEX_{86} values over the 900-3000 m depth interval (Fig. 4d) correspond to changes in reconstructed temperature of < 3 °C, which is potentially a significant difference in paleoenvironmental studies of sediments where water depth and/or bottom water ventilation have varied substantially.

5. Conclusions

Analysis of core top sediments in the Arabian Sea revealed that IPL-derived and CL-GDGT concentrations were negatively correlated to t_{OZ}, which indicates that their concentrations are dependent on preservation of fossil pelagic sources rather than in situ sedimentary production. Specific IPLs such as MH- and DH-GDGTs also showed a negative correlation with t_{OZ}. Only IPL-derived GDGT-0, as well as HPH-derived GDGTs, did not show this dependence, likely due to a contribution of in situ production in the surface sediment. Nevertheless, these in situ produced GDGTs were degraded quickly in the sediment, as concentrations of HPH-derived GDGTs at 20-24 cm sediment depth were near detection limit. TEX_{86} values of CL- and IPL-derived GDGTs decreased consistently with increasing water depth. This trend is probably not due to in situ production in the sediment. Instead, it may be due to a combination of the differential degradation of (IPL-)GDGTs and GDGTs produced in the OMZ, and a contribution of GDGTs produced in the water column at depths below 900 m. The extent of bias is not large (< 3°C over 2100 m water depth) but significant and might thus have to be accounted for, both in calibration studies and paleoclimate studies especially in areas with overlying OMZs, underlining the importance of careful sample and location selection when studying organic temperature proxies in sediment cores.

Acknowledgements. The authors would like to thank the Master and crew of the R/V Pelagia, as well as the shipboard scientific party on the PASOM cruise 2009, led by G. J. Reichart. A. Mets is thanked

for providing laboratory assistance. Three anonymous reviewers, Michael Hren and the AE Dr. Pancost, are thanked for providing constructive comments which significantly improved the manuscript. We are immensely grateful to the Darwin Center for Biogeosciences for partly financing S.K.L. by providing a grant to S.S.

452 Reference List

453

454 Agogué H., Brink M., Dinasquet J., and Herndl G. J. (2008) Major gradients inputatively nitrifying
455 and non-nitrifying Archaea in the deep North Atlantic. *Nature* **456**, 788-791.

456 Basse A., Zhu C., Versteegh G.J.M., Fischer G., Hinrichs K.-U., and Mollenhauer G. (2014)
457 Distribution of intact and core tetraether lipids in water column profiles of suspended particulate
458 matter off Cape Blanc, NW Africa. *Organic Geochemistry* **72**, 1–13.

459 Biddle J. F., Lipp J. S., Lever M. A., Lloyd K. G., Sørensen K. B., Anderson R., Fredricks H. F.,
460 Elvert M., Kelly T. J., Schrag D. P., Sogin M. L., Brenchley J. E., Teske A., House C. H., and
461 Hinrichs K.-U. (2006) Heterotrophic Archaea dominate sedimentary subsurface ecosystems off Peru.
462 *Proc. Natl. Acad. Sci. U.S.A.* **103**, 3846-3851.

463 Burd A. B., Hansell D. A., Steinberg D. K., Anderson T. R., Arístegui J., Baltar F., Beaupré S. R.,
464 Buesseler K. O., Dehairs F., Jackson G. A., Kadko D. C., Koppelmann R., Lampitt R. S., Nagata T.,
465 Reinthaler T., Robinson C., Tamburini C., and Tanaka T. (2010) Assessing the apparent imbalance
466 between geochemical and biochemical indicators of meso- and bathypelagic biological activity:
467 What the @$#! is wrong with present calculations of carbon budgets? *Deep Sea Res. Part II Top.*
468 *Stud. Oceanogr.* **57**, 1557-1571.

469 Burdige D. J. (2007) Preservation of Organic Matter in Marine Sediments: Controls, Mechanisms, and
470 an Imbalance in Sediment Organic Carbon Budgets? *Chem. Rev.* **107**, 467-485.

471 Forster A., Schouten S., Baas M., Sinninghe Damsté J.S. (2007) A mid-Cretaceous sea surface
472 temperature record of the tropical Atlantic Ocean. *Geology* **35**, 919-922.

473 Hartnett H. E., Keil R. G., Hedges J. I., and Devol A. H. (1998) Influence of oxygen exposure time on
474 organic carbon preservation in continental margin sediments. *Nature* **391**, 572-574.

475 Harvey H. R., Fallon R. D., and Patton J. S. (1986) The effect of organic matter and oxygen on the
476 degradation of bacterial membrane lipids in marine sediments. *Geochim. Cosmochim. Acta* **50**, 795-
477 804.

478 Hedges J. I., Sheng Hu F., Devol A. H., Hartnett H. E., Tsamakis E., and Keil R. G. (1999)
479 Sedimentary organic matter preservation: a test for selective degradation under oxic conditions. *Am.*
480 *J. Sci.* **299**, 529-555.

481 Herndl G. J., Reinthaler T., Teira E., van Aken H., Veth C., Pernthaler A., and Pernthaler J. (2005)
482 Contribution of *Archaea* to total prokaryotic production in the deep Atlantic Ocean. *Appl. Environ.*
483 *Microbiol.* **71**, 2303-2309.

484 Huguet C., Cartes J. E., Sinninghe Damsté J. S., and Schouten S. (2006a) Marine crenarchaeotal
485 membrane lipids in decapods: Implications for the TEX_{86} paleothermometer. *Geochem. Geophy.*
486 *Geosy.* **7**, 1-12.

487 Huguet C., Hopmans E. C., Febo-Ayala W., Thompson D. H., Sinninghe Damsté J. S., and Schouten
488 S. (2006b) An improved method to determine the absolute abundance of glycerol dibiphytanyl
489 glycerol tetraether lipids. *Org. Geochem.* **37**, 1036-1041.

490 Huguet C., Kim J.-H., de Lange G. J., Sinninghe Damsté J. S., and Schouten S. (2009) Effects of long
491 term oxic degradation on the $U^{K'}_{37}$, TEX_{86} and BIT organic proxies. *Org. Geochem.* **40**, 1188-1194.

492 Huguet C., Schimmelmann A., Thunell R., Lourens L. J., Sinninghe Damsté J. S., and Schouten S.
493 (2007) A study of the TEX_{86} paleothermometer in the water column and sediments of the Santa
494 Barbara Basin, California. *Paleoceanography* **22**, PA3203.

495 Ingalls A. E., Shah S. R., Hansman R. L., Aluwihare L. I., Santos G. M., Druffel E. R. M., and
496 Pearson A. (2006) Quantifying archaeal community autotrophy in the mesopelagic ocean using
497 natural radiocarbon. *Proc. Natl. Acad. Sci. USA* **103**, 6442-6447.

Karner M. B., DeLong E. F., and Karl D. M. (2001) Archaeal dominance in the mesopelagic zone of the Pacific Ocean. *Nature* **409**, 507-510.

Keil R. G., and Cowie G. L. (1999) Organic matter preservation through the oxygen-deficient zone of the NE Arabian Sea as discerned by organic carbon:mineral surface area ratios. *Marine Geology* **161**, 13-22.

Keil R. G., Montluçon D. B., Prahl F. G. and Hedges J. I. (1994) Sorptive preservation of labile organic matter in marine sediments. *Nature* **370**, 549-552.

Kim J.-H., Huguet C., Zonneveld K. A. F., Versteegh G. J. M., Roeder W., Sinninghe Damsté J. S., and Schouten S. (2009) An experimental field study to test the stability of lipids used for the TEX_{86} and $U^{K'}_{37}$ palaeothermometers. *Geochim. Cosmochim. Acta* **73**, 2888-2898.

Kim J.-H., Romero O. E., Lohmann G., Donner B., Laepple T., Haam E., and Sinninghe Damsté J. S. (2012) Pronounced subsurface cooling of North Atlantic waters off Northwest Africa during Dansgaard-Oescher interstadials. *Earth. Planet. Sci. Lett.* **339-340**, 95-102.

Kim J.-H., Schouten S., Hopmans E. C., Donner B., and Sinninghe Damsté J. S. (2008) Global sediment core-top calibration of the TEX_{86} paleothermometer in the ocean. *Geochim. Cosmochim. Acta* **72**, 1154-1173.

Kim J.-H., van der Meer J., Schouten S., Helmke P., Willmott V., Sangiorgi F., Koç N., Hopmans E. C., and Sinninghe Damsté J. S. (2010) New indices and calibrations derived from the distribution of crenarchaeal isoprenoid tetraether lipids: Implications for past sea surface temperature reconstructions. *Geochim. Cosmochim. Acta* **74**, 4639-4654.

Koga Y. and Nakano M. (2008) A dendrogram of archaea based on lipid component parts composition and its relationship to rRNA phylogeny. *System. Appl. Microbiol.* **31**, 169-182.

Koho K. A., Nierop K. G. J., Moodley L., Middelburg J. J., Pozzato L., Soetaert K., van der Plicht J., and Reichart G.-J. (2013) Microbial bioavailability regulates organic matter preservation in marine sediments. *Biogeosciences* **10**, 1131-1141.

Kraal P., Slomp C. P., Reed D. C., Reichart G. J., and Poulton S. W. (2012) Sedimentary phosphorus and iron cycling in and below the oxygen minimum zone of the Northern Arabian Sea. *Biogeosciences* **9**, 2603-2624.

Lengger S. K., Hopmans E. C., Reichart G.-J., Nierop K. G. J., Sinninghe Damsté J. S., and Schouten S. (2012a) Intact polar and core glycerol dibiphytanyl glycerol tetraether lipids in the Arabian Sea oxygen minimum zone: II. Selective preservation and degradation in sediments and consequences for the TEX_{86}. *Geochim. Cosmochim. Acta* **98**, 244-258.

Lengger S. K., Hopmans E. C., Sinninghe Damsté J. S., and Schouten S. (2012b) Comparison of extraction and work up techniques for analysis of core and intact polar tetraether lipids from sedimentary environments. *Org. Geochem.* **47**, 34-40.

Lengger S.K., Kraaij M., Tjallingii R., Baas M., Stuut J.-B., Hopmans E.C., Sinninghe Damsté J.S., and Schouten S. (2013) Differential degradation of intact polar and core glycerol dialkyl glycerol tetraether lipids upon post-depositional oxidation. *Org. Geochem.* **65**, 83–93.

Lin Y. S., Lipp J. S., Elvert M., Holler T., and Hinrichs K.-U. (2013) Assessing production of the ubiquitous archaeal diglycosyl tetraether lipids in marine subsurface sediment using intramolecular stable isotope probing. *Environ. Microbiol.***15**,1634-1646.

Lipp J. S. and Hinrichs K.-U. (2009) Structural diversity and fate of intact polar lipids in marine sediments. *Geochim. Cosmochim. Acta* **73**, 6816-6833.

Lipp J. S., Morono Y., Inagaki F., and Hinrichs K.-U. (2008) Significant contribution of Archaea to extant biomass in marine subsurface sediments. *Nature* **454**, 991-994.

543 Liu X., Lipp J. S., and Hinrichs K.-U. (2011) Distribution of intact and core GDGTs in marine
544 sediments. *Org. Geochem.* **42**, 368-375.

545 Liu X.-L., Lipp J. S., Simpson J. H., Lin Y. S., Summons R. E., and Hinrichs K.-U. (2012) Mono- and
546 dihydroxyl glycerol dibiphytanyl glycerol tetraethers in marine sediments: Identifications of both
547 core and intact polar lipid forms. *Geochim. Cosmochim. Acta* **89**, 102-115.

548 Liu Z., Pagani M., Zinniker D., DeConto R., Huber M., Brinkhuis H., Shah S. R., Leckie R. M., and
549 Pearson A. (2009) Global cooling during the Eocene-Oligocene climate transition. *Science* **323** ,
550 1187-1189.

551 Logemann J., Graue J., Köster J., Engelen B., Rullkötter J., and Cypionka H. (2011) A laboratory
552 experiment of intact polar lipid degradation in sandy sediments. *Biogeosciences* **8**, 2547-2560.

553 Lopes dos Santos R. A., Prange M., Castañeda I. S., Schefuß E., Mulitza S., Schulz M., Niedermeyer
554 E. M., Sinninghe Damsté J. S., and Schouten S. (2010) Glacial-interglacial variability in Atlantic
555 meridional overturning circulation and thermocline adjustments in the tropical North Atlantic. *Earth*
556 *Planet. Sci. Lett.* **300**, 407-414.

557 Middelburg J.J. (1989) A simple rate model for organic matter decomposition in marine sediments.
558 *Geochim. Cosmochim. Acta* **53**, 1577–1581.

559 Nakanishi T., Yamamoto M., Irino T., and Tada R. (2012) Distribution of glycerol dialkyl glycerol
560 tetraethers, alkenones and polyunsaturated fatty acids in suspended particulate organic matter in the
561 East China Sea. *J. Oceanogr*. **68**, 959-970.

562 Oba M., Sakata S., and Tsunogai U. (2006) Polar and neutral isopranyl glycerol ether lipids as
563 biomarkers of archaea in near-surface sediments from the Nankai. *Org. Geochem.* **37**, 1643-1654.

564 Pearson A., McNichol A. P., Benitez-Nelson B. C., Hayes J. M., and Eglinton T. I. (2001) Origins of
565 lipid biomarkers in Santa Monica Basin surface sediment: A case study using compound-specific
566 $\Delta^{14}C$ analysis. *Geochim. Cosmochim. Acta* **65**, 3123-3137.

Pitcher A., Hopmans E. C., Mosier A. C., Park S.-J., Rhee S.-K., Francis C. A., Schouten S., and Sinninghe Damsté J. S. (2011) Core and intact polar glycerol dibiphytanyl glycerol tetraether lipids of ammonia-oxidizing Archaea enriched from marine and estuarine sediments. *Appl. Environ. Microbiol.* **77**, 3468-3477.

Pitcher A., Hopmans E. C., Schouten S., and Sinninghe Damsté J. S. (2009) Separation of core and intact polar archaeal tetraether lipids using silica columns: Insights into living and fossil biomass contributions. *Org. Geochem.* **40**, 12-19.

Pitcher A., Rychlik N., Hopmans E. C., Spieck E., Rijpstra W. I. C., Ossebaar J., Schouten S., Wagner M., and Sinninghe Damsté J. S. (2010) Crenarchaeol dominates the membrane lipids of *Candidatus* Nitrososphaera gargensis, a thermophilic Group I.1b Archaeon. *ISME J* **4**, 542-552.

Reinthaler T., van Aken H. M., and Herndl G. J. (2010) Major contribution of autotrophy to microbial carbon cycling in the deep North Atlantic's interior. *Deep Sea Res. Part II Top. Stud. Oceanogr.* **57**, 1572-1580.

Revsbech N. P. (1989) An oxygen microsensor with a guard cathode. *Limnol. Oceanogr.* **34**, 474-478.

Schouten S., Hopmans E. C., Baas M., Boumann H., Standfest S., Könneke M., Stahl D. A., and Sinninghe Damsté J. S. (2008) Intact membrane lipids of "*Candidatus* Nitrosopumilus maritimus," a cultivated representative of the cosmopolitan mesophilic group I crenarchaeota. *Appl. Environ. Microbiol.* **74**, 2433-2440.

Schouten S., Hopmans E. C., Schefuß E., and Sinninghe Damsté J. S. (2002) Distributional variations in marine crenarchaeotal membrane lipids: a new tool for reconstructing ancient sea water temperatures? *Earth. Planet. Sci. Lett.* **204**, 265-274.

Schouten S., Hopmans E. C., and Sinninghe Damsté J. S. (2004) The effect of maturity and depositional redox conditions on archaeal tetraether lipid palaeothermometry. *Org. Geochem.* **35**, 567-571.

591 Schouten S., Huguet C., Hopmans E. C., Kienhuis M. V. M., and Sinninghe Damsté J. S. (2007)
592 Analytical Methodology for TEX_{86} Paleothermometry by High-Performance Liquid Chromatography
593 / Atmospheric Pressure Chemical Ionization-Mass Spectrometry. *Anal. Chem.* **79**, 2940-2944.

594 Schouten S., Middelburg J. J., Hopmans E. C., and Sinninghe Damsté J. S. (2010) Fossilization and
595 degradation of intact polar lipids in deep subsurface sediments: A theoretical approach. *Geochim.*
596 *Cosmochim. Acta* **74**, 3806-3814.

597 Schouten S., Pitcher A., Hopmans E. C., Villanueva L., van Bleijswijk J., and Sinninghe Damsté J. S.
598 (2012) Intact polar and core glycerol dibiphytanyl glycerol tetraether lipids in the Arabian Sea
599 oxygen minimum zone: I. Selective preservation and degradation in the water column and
600 consequences for the TEX_{86}. *Geochim. Cosmochim. Acta* **98**, 228-243.

601 Schubotz F., Wakeham S. G., Lipp J. S., Fredricks H. F., and Hinrichs K.-U. (2009) Detection of
602 microbial biomass by intact polar membrane lipid analysis in the water column and surface
603 sediments of the Black Sea. *Environ. Microbiol.* **11**, 2720-2734.

604 Shah S. R., Mollenhauer G., Ohkouchi N., Eglinton T., and Pearson A. (2008) Origins of archaeal
605 tetraether lipids in sediments: Insights from radiocarbon analysis. *Geochim. Cosmochim. Acta* **72**,
606 4577-4594.

607 Sinninghe Damsté J. S., Rijpstra W. I. C., Hopmans E. C., Prahl F. G., Wakeham S. G., and Schouten
608 S. (2002a) Distribution of membrane lipids of planktonic *Crenarchaeota* in the Arabian Sea. *Appl.*
609 *Environ. Microbiol.* **68**, 2997-3002.

610 Sinninghe Damsté J. S., Rijpstra W. I. C., and Reichart G.-J. (2002b) The influence of oxic
611 degradation on the sedimentary biomarker record II. Evidence from Arabian Sea sediments.
612 *Geochim. Cosmochim. Acta* **66**, 2737-2754.

613 Sinninghe Damsté J. S., Schouten S., Hopmans E. C., van Duin A. C. T., and Geenevasen J. A. J.
614 (2002c) Crenarchaeol: the characteristic core glycerol dibiphytanyl glycerol tetraether membrane
615 lipid of cosmopolitan pelagic crenarchaeota. *J. Lipid Res.* **43**, 1641-1651.

Taylor K.W.R., Huber M., Hollis C.J., Hernandez-Sanchez M.T., and Pancost R.D. (2013) Re-evaluating modern and Palaeogene GDGT distributions: Implications for SST reconstructions. *Global and Planetary Change* **108**, 158–174.

Turich C., Freeman K. H., Bruns M. A., Conte M., Jones A. D., and Wakeham S. G. (2007) Lipids of marine Archaea: Patterns and provenance in the water-column and sediments. *Geochim. Cosmochim. Acta* **71**, 3272-3291.

Wakeham S. G., Lewis C. M., Hopmans E. C., Schouten S., and Sinninghe Damsté J. S. (2003) Archaea mediate anaerobic oxidation of methane in deep euxinic waters of the Black Sea. *Geochim. Cosmochim. Acta* **67**, 1359-1374.

Wuchter C., Schouten S., Wakeham S. G., and Sinninghe Damsté J. S. (2005) Temporal and spatial variation in tetraether membrane lipids of marine Crenarchaeota in particulate organic matter: Implications for TEX_{86} paleothermometry. *Paleoceanography* **20**, PA3013.

Wuchter C., Schouten S., Wakeham S. G., and Sinninghe Damsté J. S. (2006) Archaeal tetraether membrane lipid fluxes in the northeastern Pacific and the Arabian Sea: Implications for TEX_{86} paleothermometry. *Paleoceanography* **21**, PA4208.

Xie S., Lipp J. S., Wegener G., Ferdelman T. G., and Hinrichs K.-U. (2013) Turnover of microbial lipids in the deep biosphere and growth of benthic archaeal populations. *Proc. Natl. Acd. Sci. USA*, **110**, 6010-6014.

635 Figure captions.

636 Figure 1. Structures of CL-GDGTs (a) and IPL-GDGTs isolated by semi-preparative HPLC (b).

637 Figure 2. Map of the Murray Ridge in the North Arabian Sea with sampling stations indicated.
638 Underwater topography is shown as 100 m contour lines.

639 Figure 3. Characteristics of the surface sediment. Bottom water oxygen concentrations (a) maximum
640 residence time in the oxic zone (t_{OZ}) of the top 0.5 cm (as calculated from sedimentation rates and
641 oxygen penetration depths (b) and organic carbon content (c) of the surface (0.5 cm) sediments of the
642 Murray Ridge plotted vs. water depth

643 Figure 4. Changes in GDGTs in core tops (0-0.5 cm) with water depth at which the sediment was
644 retrieved. Core lipid-GDGT concentrations (a), IPL-derived GDGT concentrations (b) and %IPL of
645 total GDGTs (c) in surface (0-0.5 cm) sediments, (d) TEX_{86} values of the surface sediment of CL-,
646 IPL- and ASE-extracted GDGTs plotted versus water depth.

647 Figure 5. Results of the semi-preparative HPLC. (a) Amounts of different GDGTs (GDGT-0,
648 crenarchaeol, and other isoprenoid GDGTs) in the IPLs (i.e. MH, DH and HPH) isolated by semi-
649 preparative HPLC in the surface (0-2 cm) and deeper (20-24 cm) of stations P900, P1300, and P3000
650 (Left panels). GDGT distributions of the different isolated IPLs are shown in the right panels. (b)
651 shows the TEX_{86} values of IPL-fractions (MH-, DH- and HPH-GDGTs) at the three stations and two
652 sediment depths, and the combined TEX_{86} values of those fractions isolated by semi-preparative
653 HPLC ("total"). For comparison, the TEX_{86} values at these stations, measured by separating IPL-
654 GDGTs using silica column chromatography are shown ("IPL-derived"). For 0-2 cm, weighted
655 averages were calculated from data published by Lengger et al. (2012a), for 20-24 cm, values shown
656 ibid were used.

657 Figure 6. Correlations with maximum residence time in the oxic zone (t_{OZ}). (a) C_{org}, (b) TEX_{86}, (c) CL-
658 GDGT concentrations and (d) IPL-derived GDGT concentrations.

Table

Table 1. Organic carbon content (C_{org}), bottom water oxygen concentration (BWO), oxygen penetration depth (OPD) and sedimentation rates as well as maximum residence time in the oxic zone (t_{OZ}) of surface (0-0.5 cm) sediments deposited at stations from a different water depths.

Station	**Water depth** [m]	**C_{org}** [mg . g sed dw^{-1}]	**BWO**[b] [µmol . L^{-1}]	**OPD** [mm]	**Sed. rate** [mm . kyr^{-1}]	**t_{OZ}** [yr]
P900	885	60.6	2.1	0.1	134[a]	1
P1000	1013	46.3	2.6	1.0	40[b]	25
P1200	1172	41.2	5.1	1.4	22[b]	63
P1300	1306	24.9	13.8	2.9	38[a]	77
P1400	1379	11.4	16.8	5.8	33[b]	152
P1500	1495	12.4	26.8	7.1	n.d.[c]	n.d.[c]
P1800	1786	12.1	45.2	6.2	30[b]	167
P2000	1970	8.6	56.9	5.8	26[b]	192
P2500	2470	9.8	66.3	9.8	26[b]	192
P3000	3003	7.0	76.9	19.0	83[a,d]	60

[a] Lengger et al., 2012

[b] Koho et al., 2013

[c] Values could not be determined.

[d] This value is likely overestimated due to of lateral transport.

Table 2. Degradation constants, i.e. slopes relative to initial concentrations for C_{org}, core lipid (CL)- and intact polar lipid (IPL)-derived GDGTs.

		C_0 **µg . g sed dw^{-1}**	**k** **yr^{-1}**	**k/C_0** **µg . g sed dw . yr^{-1}**	**R^2**	**P**
	C_{org}	5.4 ± 0.4	0.025 ± 0.003	0.46	0.93	0.0001
CL	Crenarchaeol	53 ± 7	0.28 ± 0.005	0.54	0.82	0.002
	GDGT-0	7.4 ± 0.9	0.037 ± 0.007	0.50	0.80	0.0016
	Minor i-GDGTs	14 ± 2	0.075 ± 0.014	0.53	0.80	0.0016
IPL	Crenarchaeol	3.0 ± 0.3	0.014 ± 0.002	0.45	0.86	0.0005
	GDGT-0	0.98 ± 0.13	0.0025 ± 0.0010	0.25	0.49	0.0538
	Minor i-GDGTs	1.5 ± 0.2	0.0074 ± 0.0011	0.49	0.85	0.0006

Figure

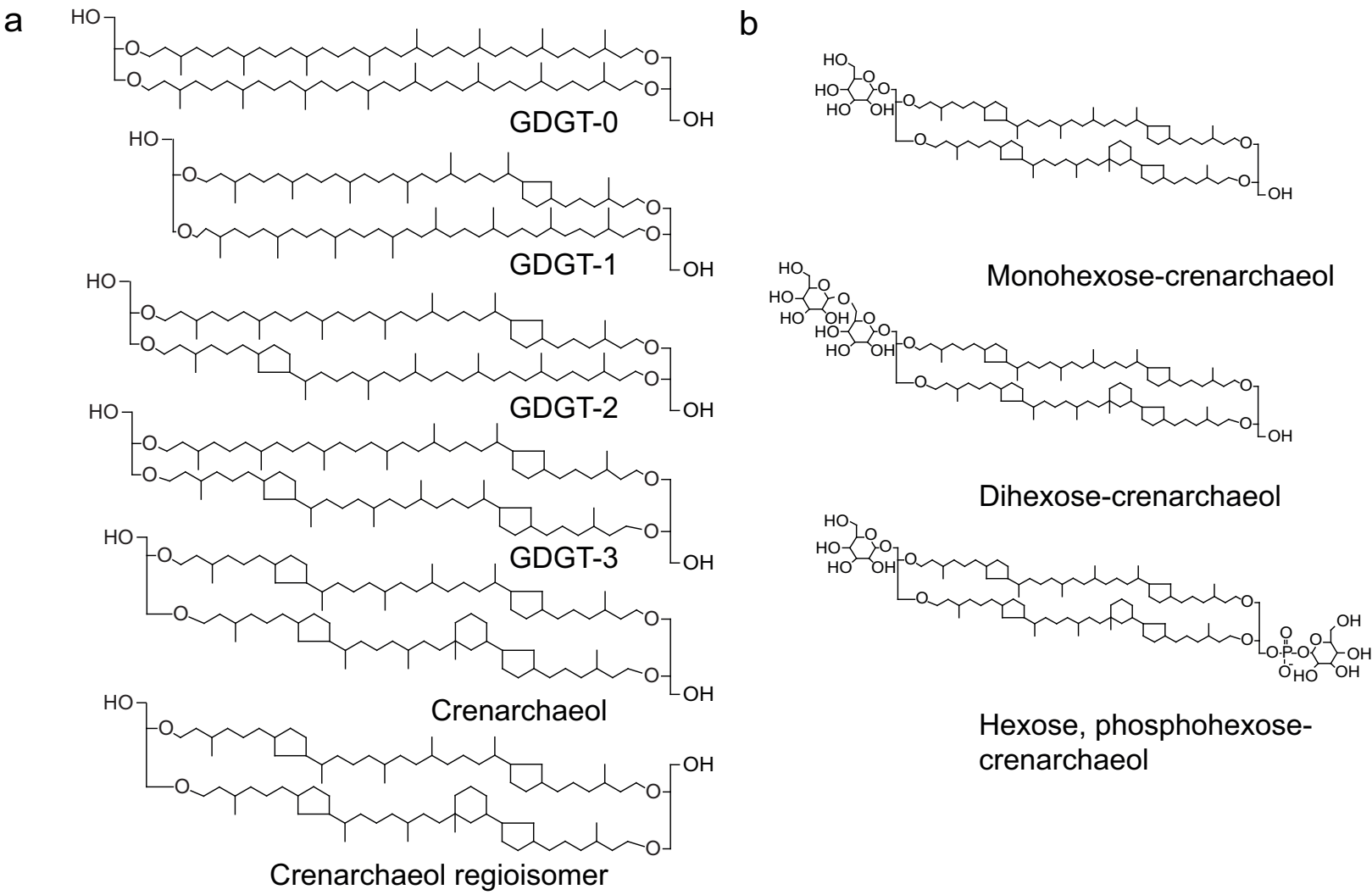
a
GDGT-0
GDGT-1
GDGT-2
GDGT-3
Crenarchaeol
Crenarchaeol regioisomer
b
Monohexose-crenarchaeol
Dihexose-crenarchaeol
Hexose, phosphohexose-crenarchaeol

Figure

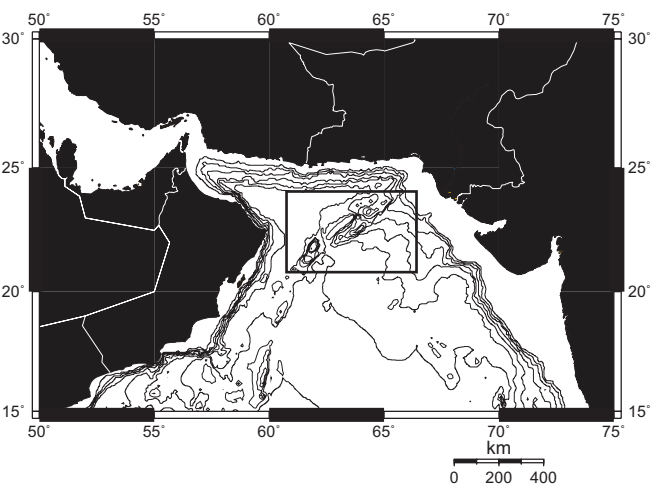
50˚
55˚
60˚
65˚
70˚
75˚
30˚
25˚
20˚
15˚
km
0 200 400

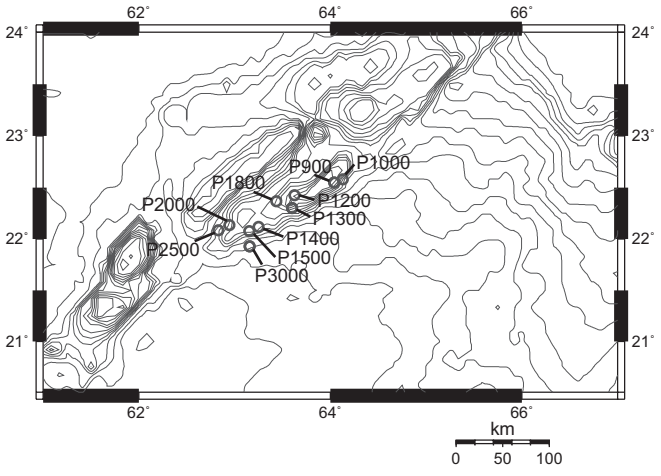
62˚
64˚
66˚
24˚
23˚
22˚
21˚
P900
P1000
P1800
P2000
P1200
P1300
P1400
P2500
P1500
P3000
km
0 50 100

Figure

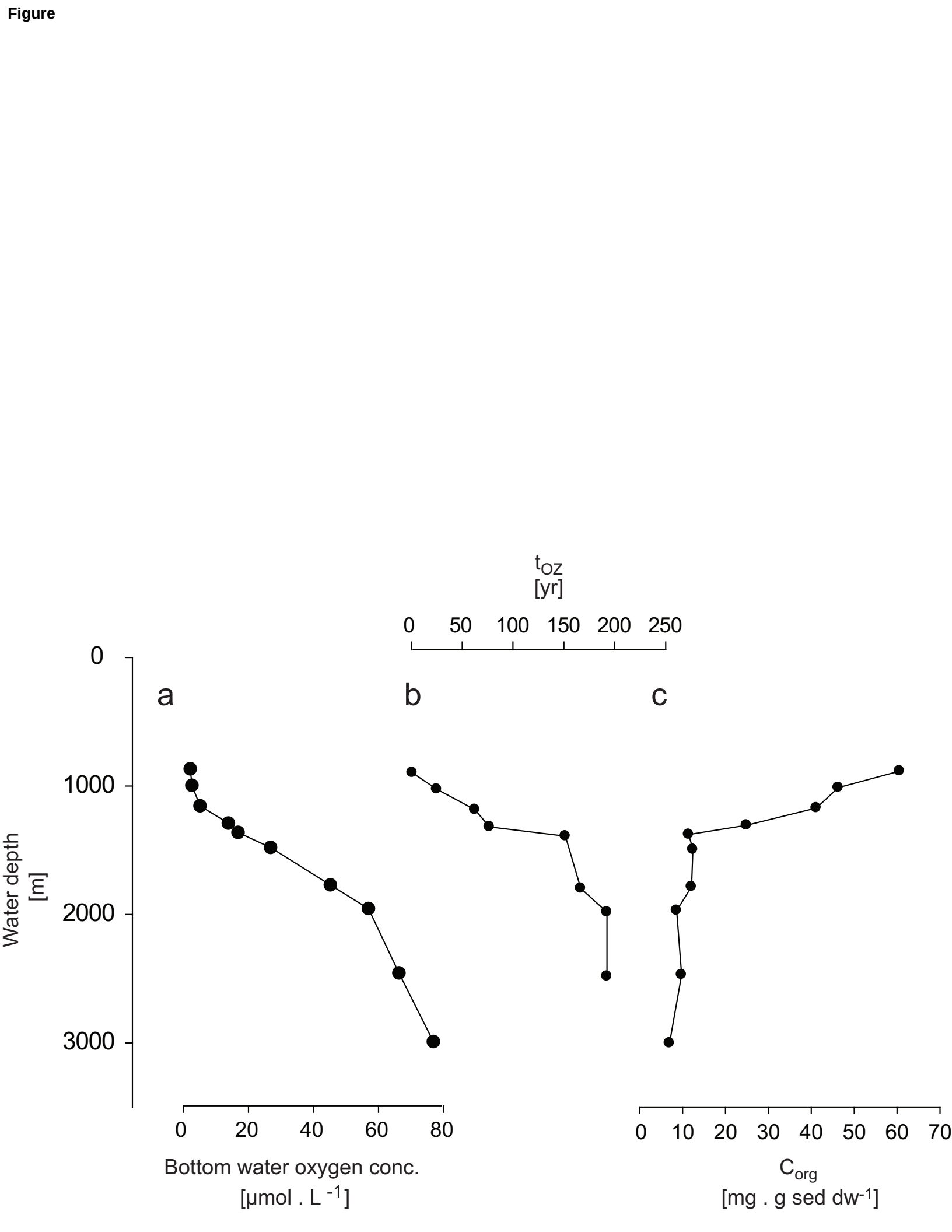
t_{OZ}
[yr]
0
50
100
150
200
250
a
b
c
0
1000
2000
3000
Water depth
[m]
0
20
40
60
80
Bottom water oxygen conc.
[µmol . L $^{-1}$]
0
10
20
30
40
50
60
70
C_{org}
[mg . g sed dw^{-1}]

Figure

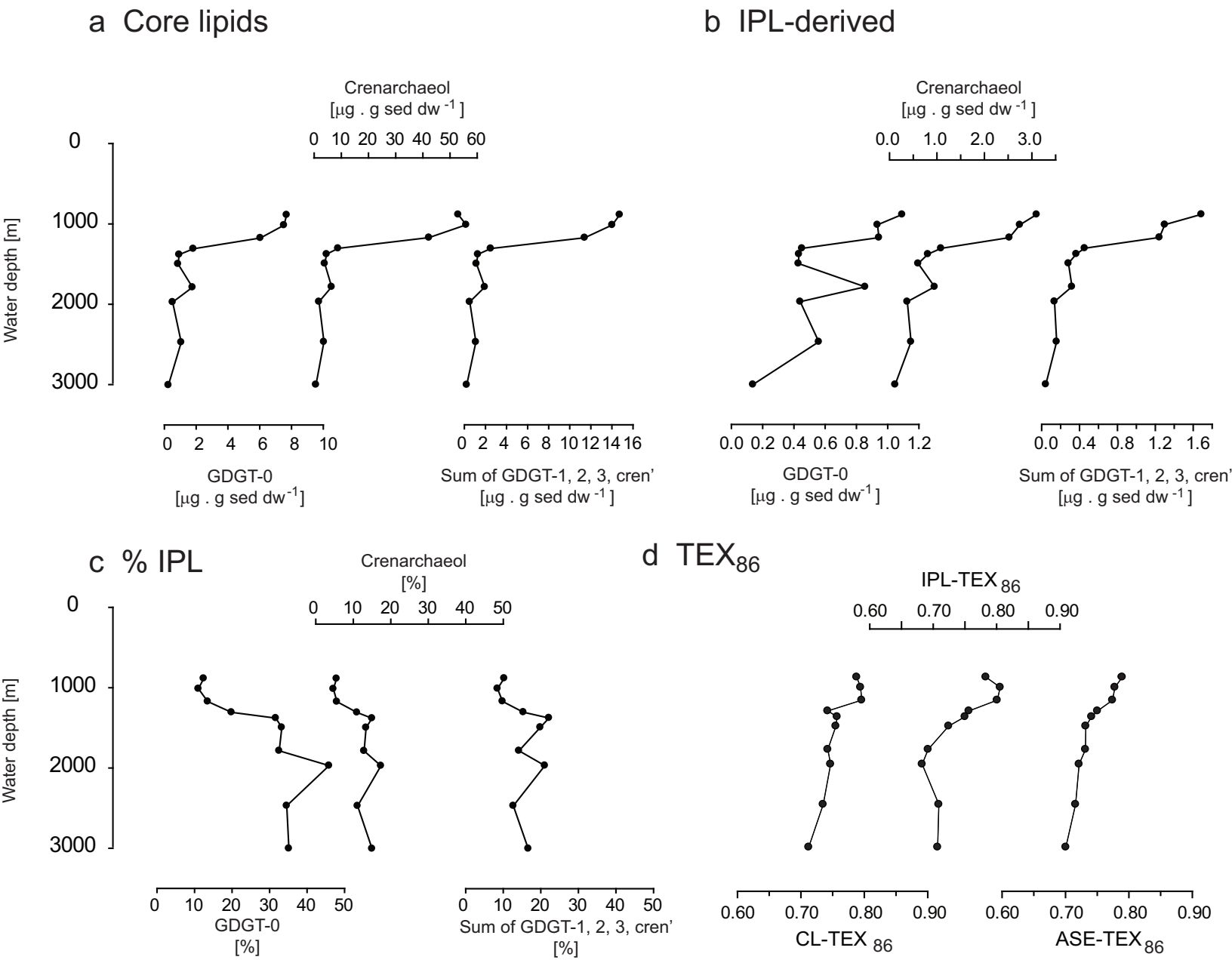
a Core lipids
b IPL-derived
c % IPL
d TEX86
Water depth [m]
0
1000
2000
3000
Crenarchaeol
[µg . g sed dw -1]
0 10 20 30 40 50 60
0.0 1.0 2.0 3.0
GDGT-0
[µg . g sed dw-1]
0 2 4 6 8 10
0.0 0.2 0.4 0.6 0.8 1.0 1.2
Sum of GDGT-1, 2, 3, cren'
[µg . g sed dw -1]
0 2 4 6 8 10 12 14 16
0.0 0.4 0.8 1.2 1.6
Crenarchaeol
[%]
0 10 20 30 40 50
GDGT-0
[%]
0 10 20 30 40 50
Sum of GDGT-1, 2, 3, cren'
[%]
0 10 20 30 40 50
IPL-TEX 86
0.60 0.70 0.80 0.90
CL-TEX 86
0.60 0.70 0.80 0.90
ASE-TEX86
0.60 0.70 0.80 0.90

Figure

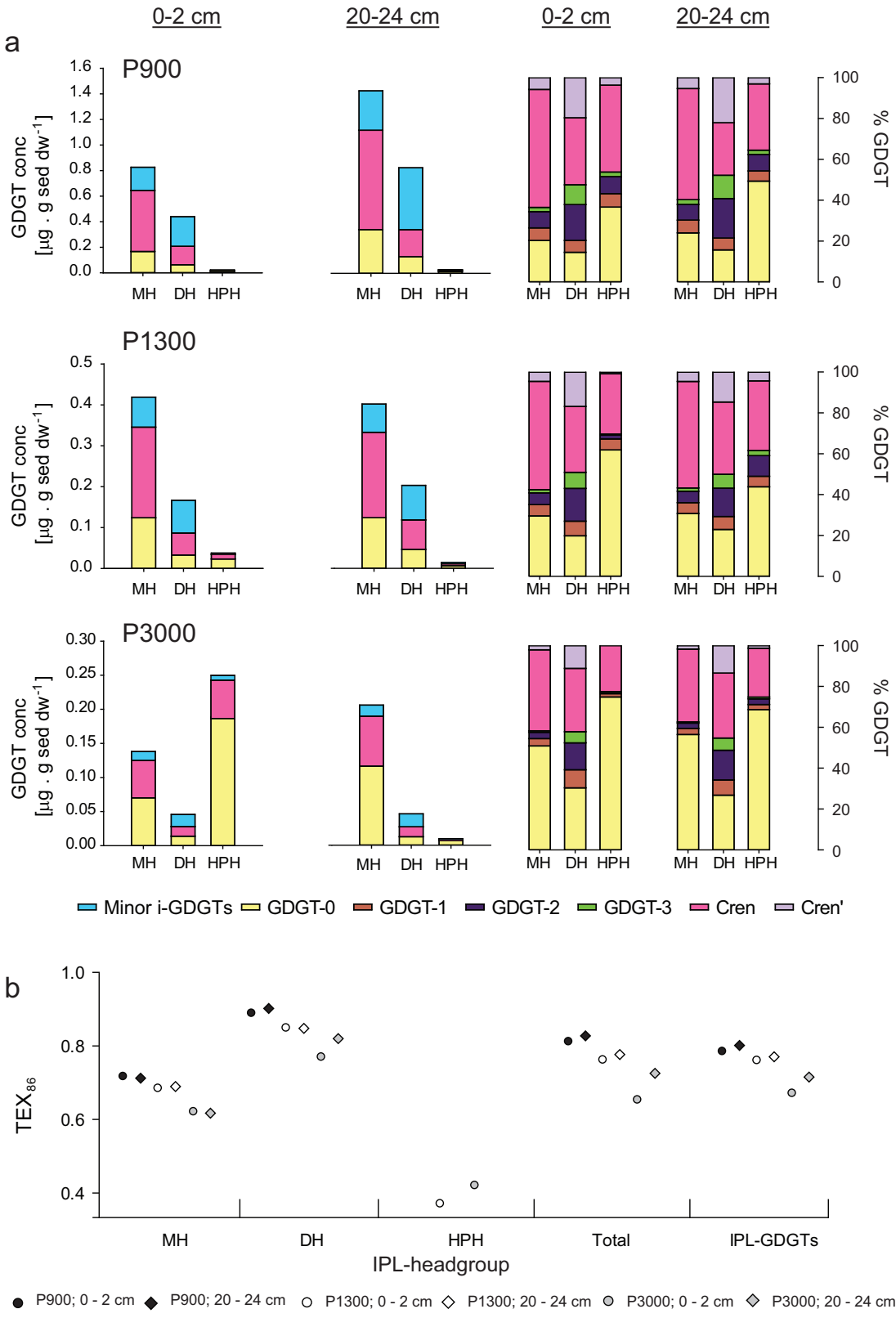
a
0-2 cm
20-24 cm
0-2 cm
20-24 cm
P900
P1300
P3000
GDGT conc [µg . g sed dw-1]
% GDGT
MH DH HPH
Minor i-GDGTs
GDGT-0
GDGT-1
GDGT-2
GDGT-3
Cren
Cren'
b
TEX86
IPL-headgroup
MH
DH
HPH
Total
IPL-GDGTs
P900; 0 - 2 cm
P900; 20 - 24 cm
P1300; 0 - 2 cm
P1300; 20 - 24 cm
P3000; 0 - 2 cm
P3000; 20 - 24 cm

Figure

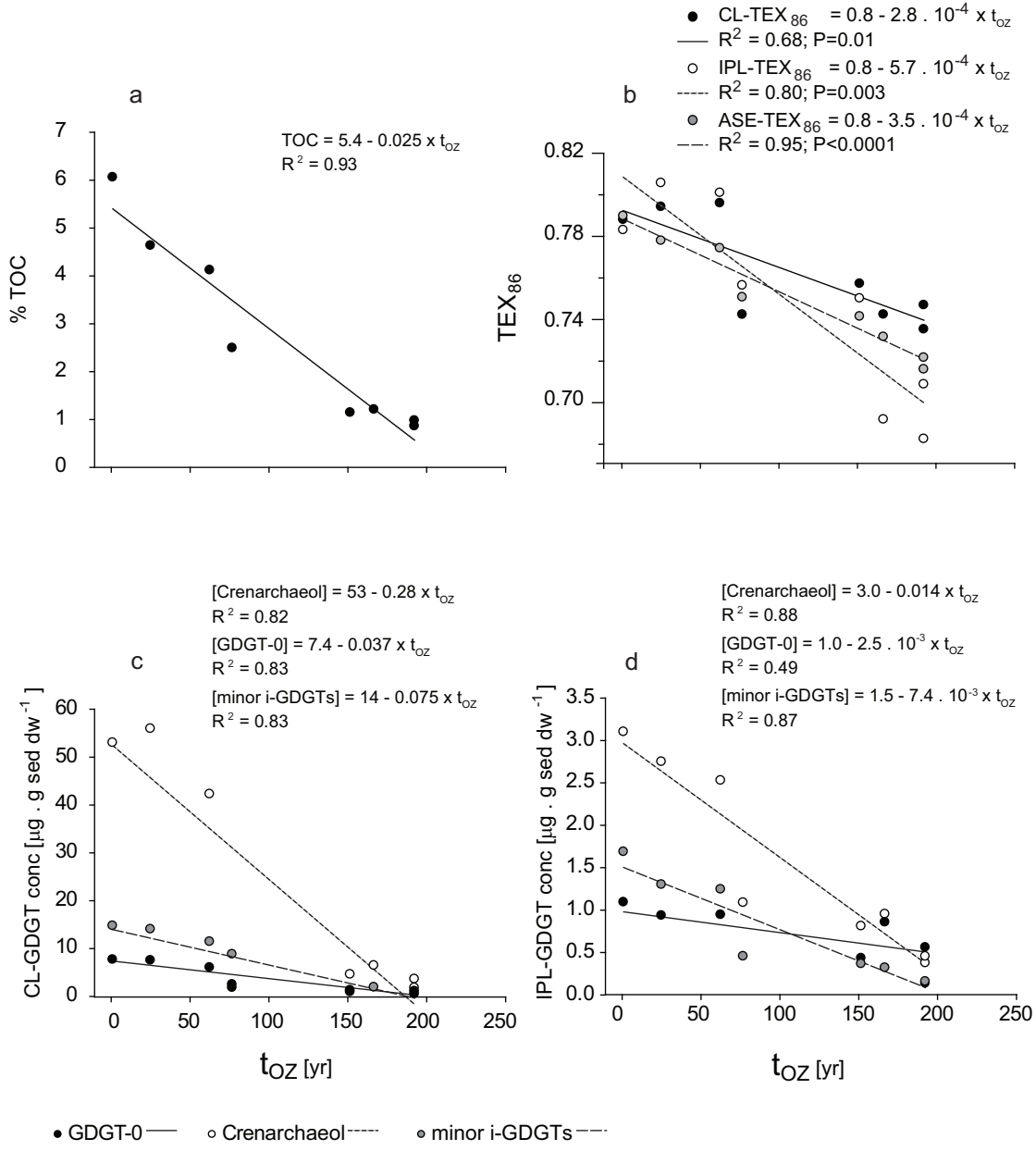

GDGT-0 Crenarchaeol minor i-GDGTs

Figure 6.

Appendix

Click here to download Appendix: Table A1_2.docx

Appendix

Click here to download Appendix: Table A2.docx

Appendix

Click here to download Appendix: Table A3_2.docx